HHS Public Access

Author manuscript

Ecotoxicol Environ Saf. Author manuscript; available in PMC 2025 May 13.

Published in final edited form as:

Ecotoxicol Environ Saf. 2024 June 15; 278: 116423. doi:10.1016/j.ecoenv.2024.116423.

$PM_{2.5}$-induced cellular senescence drives brown adipose tissue impairment in middle-aged mice

Renjie Hu[a,b,1], **Wenjun Fan**[a,1], **Sanduo Li**[a,1], **Guoqing Zhang**[a,b], **Lu Zang**[a,b], **Li Qin**[a,b], **Ran Li**[a,b], **Rucheng Chen**[a,b], **Lu Zhang**[a,b], **Weijia Gu**[a,b], **Yunhui Zhang**[c], **Sanjay Rajagopalan**[d], **Qinghua Sun**[a,b], **Cuiqing Liu**[a,b,*]

[a]School of Public Health, Zhejiang Chinese Medical University, Hangzhou 310053, China

[b]Zhejiang International Science and Technology Cooperation Base of Air Pollution and Health, Hangzhou 310053, China

[c]Key Laboratory of Public Health Safety, Ministry of Education, School of Public Health, Fudan University, Shanghai 200433, China

[d]School of Medicine, Case Western Reserve University, Cleveland, OH 44106, USA

Abstract

Airborne fine particulate matter ($PM_{2.5}$) exposure is closely associated with metabolic disturbance, in which brown adipose tissue (BAT) is one of the main contributing organs. However, knowledge of the phenotype and mechanism of $PM_{2.5}$ exposure-impaired BAT is quite limited. In the study, male C57BL/6 mice at three different life phases (young, adult, and middle-aged) were simultaneously exposed to concentrated ambient $PM_{2.5}$ or filtered air for 8 weeks using a whole-body inhalational exposure system. H&E staining and high-resolution respirometry were used to assess the size of adipocytes and mitochondrial function. Transcriptomics was performed to determine the differentially expressed genes in BAT. Quantitative RT-PCR, immunohistochemistry staining, and immunoblots were performed to verify the transcriptomics and explore the mechanism for BAT mitochondrial dysfunction. Firstly, $PM_{2.5}$ exposure caused altered BAT morphology and mitochondrial dysfunction in middle-aged but not young or adult mice. Furthermore, $PM_{2.5}$ exposure increased cellular senescence in BAT of middle-aged mice, accompanied by cell cycle arrest, impaired DNA replication, and inhibited AKT signaling pathway. Moreover, $PM_{2.5}$ exposure disrupted apoptosis and autophagy homeostasis in BAT of

*Correspondence to: School of Public Health, Zhejiang Chinese Medical University, 548 Binwen Rd, Hangzhou 310053, China, liucuiqing@zcmu.edu.cn (C. Liu).

[1]These authors contributed equally.

CRediT authorship contribution statement

Weijia Gu: Investigation. **Yunhui Zhang:** Writing – review & editing. **Rucheng Chen:** Formal analysis. **Lu Zhang:** Investigation. **Cuiqing Liu:** Writing – review & editing, Supervision, Project administration, Funding acquisition, Conceptualization. **Sanjay Rajagopalan:** Writing – review & editing. **Qinghua Sun:** Writing – review & editing. **Wenjun Fan:** Writing – original draft, Visualization, Investigation, Formal analysis. **Sanduo Li:** Writing – original draft, Visualization, Investigation, Formal analysis. **Renjie Hu:** Writing – original draft, Visualization, Investigation, Formal analysis. **Li Qin:** Investigation. **Ran Li:** Investigation. **Guoqing Zhang:** Investigation. **Lu Zang:** Investigation.

Declaration of Competing Interest

The authors declare that they have no known competing financial interests or personal relationships that could have appeared to influence the work reported in this paper.

middle-aged mice. Therefore, BAT in middle-aged mice was more vulnerable to $PM_{2.5}$ exposure, and the cellular senescence-initiated apoptosis, autophagy, and mitochondrial dysfunction may be the mechanism of $PM_{2.5}$ exposure-induced BAT impairment.

Keywords

Fine particulate matter; Brown adipose tissue; Cellular senescence; Mitochondrial dysfunction; Apoptosis; Autophagy

1. Introduction

Air pollution has been a rising global health threat over several decades, particularly in developing countries (Araviiskaia et al., 2019; GBD 2015 Risk Factors Collaborators, 2016). As the most harmful component of air pollutants, airborne fine particulate matter ([$PM_{2.5}$], aerodynamic diameter ≤ 2.5 μm) is composed of carbonaceous nuclei with adsorbed organic and inorganic reactive chemicals (Della Guardia and Shin, 2022a; Liang et al., 2016). It is associated with metabolic syndrome containing central obesity, dyslipidemia, hypertension, and increased fasting glucose (Li et al., 2023; Yi et al., 2022). In the patho-physiology of the metabolic syndrome, adipose tissues, the largest and most active endocrine organ that performs metabolic and immune functions, are of great concern (Torres et al., 2019; Wang et al., 2022b). Of all adipose tissue types, brown adipose tissue (BAT) is crucial in protecting from diet-induced obesity and energy metabolic dysfunction (Hamann et al., 1996). Our previous work showed that male mice at 12 months of age (middle-aged) were more vulnerable to the impact of $PM_{2.5}$ exposure on hepatic lipid metabolism compared to mice at 3 weeks of age (young) and 8 weeks of age (adult) (Hu et al., 2023). However, very limited studies have suggested that exposure to $PM_{2.5}$ reduced mitochondrial size in BAT of adult mice (Xu et al., 2011). The detailed effect of $PM_{2.5}$ exposure on BAT, its age susceptibility, and the underlying molecular mechanisms are still not understood in detail.

Many studies have implicated cell senescence in metabolic syndrome (Khosla et al., 2020; Wiley and Campisi, 2021). Cell senescence is characterized by cell cycle arrest and impaired DNA replication (Herranz and Gil, 2018; Martin and Wood, 2019). In addition, senescent cells also undergo a number of phenotypic changes, including metabolic reprogramming and cell death regulation (Herranz and Gil, 2018). Apoptosis, known as self-killing, is a type of programmed cell death, while autophagy involves lysosomal degradation. They are essential for cell death, and their homeostasis is basic for cell function (Vicencio et al., 2008). Although recent studies have indicated that $PM_{2.5}$ exposure accelerated cellular senescence and activated apoptotic pathways in lung, vascular smooth muscle cells, skin keratinocytes, and endothelial cells (Gu et al., 2022; Kang et al., 2023; Sharma et al., 2019; Wang et al., 2022a; Zhang et al., 2021), whether they are involved in BAT impairment caused by $PM_{2.5}$ exposure remains to be understood.

Therefore, in this study, our hypothesis is that $PM_{2.5}$ exposure could cause cell cycle arrest and cell senescence in BAT of middle-aged male mice, with disruption of apoptosis and autophagy homeostasis, ultimately causing BAT metabolic dysfunction. This study offers valuable insights into $PM_{2.5}$-induced BAT dysfunction from the perspective of cellular

senescence, which provides an experimental basis to counter metabolic disorders induced by $PM_{2.5}$.

2. Materials and methods

2.1. Animal care and use

C57BL/6 male mice at different ages, 3 weeks (young), 8 weeks (adults), and 12 months (middle-aged) old, were purchased from Charles River Laboratories (Beijing, China). All mice were housed in a constant temperature environment (22 ± 2°C) with a 12-hour light and 12-hour dark cycle with ad libitum access to diet and water. The Institutional Animal Care and Use Committee of Zhejiang Chinese Medical University (ZCMU) authorized all animal-related experiments performed in this study.

2.2. Whole-body inhalation exposure protocol

Mice in each age group were randomly assigned to two groups and simultaneously exposed to filtered air (FA) and concentrated $PM_{2.5}$ using a whole-body inhalation exposure system situated at ZCMU. The exposure regimen is as follows: 12 h/day, 6 days/week, for 8 weeks. The working principles of the exposure system have been described in a previous study (Hu et al., 2023). Briefly, to obtain filtered air, the air inlet of the FA chamber is fitted with a HEPA filter to remove particles present in the ambient air. For concentrated $PM_{2.5}$, a cyclone device is first used to obtain $PM_{2.5}$ from the ambient air, and then a series of virtual impactors are used to concentrate $PM_{2.5}$ and finally pass it into the $PM_{2.5}$ chamber at a constant flow rate. Mice were provided with food and water during the exposure process.

2.3. Tissue collection

After eight-week $PM_{2.5}$ exposure, all mice were euthanized to collect and weigh BAT, inguinal white adipose tissue (iWAT), and visceral adipose tissue (VAT). To avoid sampling errors, we selected the same site of BAT for each experiment and avoided using the interface between BAT and white adipose tissue. The BAT was divided into three parts immediately after it was separated from each mouse: one part was immediately homogenized on ice for mitochondrial function determination, one part was placed in paraformaldehyde for paraffin embedding, and the remaining part was quickly frozen in liquid nitrogen, and then stored in a −80°C refrigerator for subsequent experiments.

2.4. High-resolution respirometry

The isolated BAT was immediately submerged in MiR05 medium (10 mM KH_2PO_4, 3 mM $MgCl_2 \cdot 6\ H_2O$, 0.5 mM EGTA, 110 mM D-Sucrose, 20 mM HEPES, and 20 mM Taurine) and homogenized on ice. The homogenate was moved to the chambers of O2k (OROBOROS instruments, Innsbruck, Austria) to detect O_2 flux, which was monitored on the Oroboros Datlab software (OROBOROS instruments, Innsbruck, Austria).

O2k manual titration scheme is as follows: 1) complex I LEAK respiration (CI_L) was determined by adding 5 mM pyruvate (P2256, Sigma), 10 mM glutamate (49621, Sigma), and 2 mM malate (M1125, Sigma); 2) the OXPHOS capacity of Complex I (CI_P) was measured by injecting 1 mM ADP (A2754, Sigma); 3) the integrity of mt-outer membrane

was checked by injecting 10 μM Cyt. *c* (C7752, Sigma); 4) the OXPHOS capacity of Complex I and II ($CI\&II_P$) was measured by adding 10 mM succinate (S9637, Sigma); 5) the electron transfer system (ETS) capacity of Complex I and II ($CI\&II_E$) was measured by adding 0.5 μM FCCP (C2920, Sigma); 6) the ETS capacity of Complex II (CII_E) was measured by adding 0.5 μM rotenone (R8875, Sigma), an inhibitor of Complex I; 7) after inhibition of Complex III with 2.5 μM Antimycin A (A8674, Sigma), the Complex IV respiratory was detected by adding 2 mM ascorbate (PHR1279, Sigma) and 0.5 mM TMPD (T3134, Sigma). O_2 flux was calibrated by tissue mass.

2.5. Histology analysis

Paraffin-embedded BAT was prepared into 5-micron sections for histology analysis. The H&E staining protocol was executed as described previously (Hu et al., 2023). The average adipocyte size was analyzed using Image J 1.6.0 (four randomly selected fields per section were averaged).

Immunohistochemistry staining was performed with an SP link Detection Kit (KIT-9710, MXB Biotechnologies, China), and the protocol was described previously (Fan et al., 2023). Briefly, after deparaffinization and rehydration, sections were subjected to antigen retrieval with Tris-EDTA solution (PR30002, Proteintech, China) at 98°C for 10 min, incubated in H_2O_2 for 10 min, and then blocked with non-specific staining inhibitors for 20 min. Then, the sections were treated with primary antibody beta-galactosidase (β-Gal) antibody (1:100; Cat# 15518–1-AP; Proteintech) and incubated overnight at 4°C. Following the washing step, the sections were incubated with secondary antibodies, followed by diaminobenzidine (ZLI-9018, ZSGB-Biotech). The sections were restained using an immunohistochemistry autostainer (Autostainer480, Thermo Fisher Scientific, USA). The positive area was analyzed using Image J 1.6.0 (five randomly selected fields per section were averaged).

2.6. Transcriptomics and data analysis

As indicated previously, transcriptomic sequencing was performed by Novogene Co. Ltd. (Beijing) (Hu et al., 2023). The thresholds for identifying differentially expressed genes (DEGs) were adjusted as $P \leq 0.05$ and $|\log_2\text{Fold Change}| \geq 1$. GraphPad Prism 8.0 and TBtools software (Chen et al., 2020) were utilized to generate volcano plots and heatmaps, respectively.

For enrichment analysis of transcriptome data, the Novomagic platform (https://magic.novogene.com) was used to perform gene Ontology (GO) and the Kyoto Encyclopedia of Genes and Genomes (KEGG) enrichment analyses. Gene set enrichment analysis (GSEA) software version 4.21 was utilized to perform GSEA (Subramanian et al., 2005).

For analyzing protein-protein interaction (PPI), we utilized the STRING database (https://cn.string-db.org) to predict potential protein interaction pairs, which were then visualized using Cytoscape (Shannon et al., 2003). The Molecular Complex Detection (MCODE) and CytoHubba plugin in Cytoscape were utilized to calculate essential modules and the hub genes in the PPI network, respectively (Bader and Hogue, 2003).

2.7. mRNA expression analysis

Following the extraction of total RNA from BAT using RNAiso Plus (TaKaRa, Shiga, Japan), the synthesis of cDNA was performed using PrimeScript RT Master Mix (TaKaRa, Shiga, Japan). The procedure of quantitative real-time PCR (qRT-PCR) was run on a QuantStudio 7 Flex instrument(Applied Biosystems, USA) using PowerUP SYBR Green Master Mix (Applied Biosystems, USA) as the fluorescent dye as described previously (Hu et al., 2023). Glyceraldehyde-3-phosphate dehydrogenase (*Gapdh*) was used to standardize mRNA expression levels. The primer sequences are provided in Table 1.

2.8. Immunoblotting

Following the extraction of total protein from BAT using RIPA lysis buffer (Boster, California, US), the protein levels were detected with the BCA Protein Assay Kit (Beyotime Biotech., Shanghai, China). Immunoblotting was performed as described in previous studies (Hu et al., 2023). After electrophoresis, the proteins were transferred to a PVDF membrane and then blocked using 5% BSA. Subsequently, the membrane underwent overnight incubation at a temperature of 4°C with the primary antibodies, including β-Gal antibody (1:1000; Cat# 15518–1-AP; Proteintech), protein kinase B (AKT) antibody (1:1000; Cat# 9272; Cell Signaling Technology), pAKT antibody (phosphorylated at Ser473; 1:1000; Cat# 4060; Cell Signaling Technology), LC3I/II antibody (1:1000; Cat# 12741; Cell Signaling Technology), autophagy related 5 (ATG5) antibody (1:1000; Cat# 12994; Cell Signaling Technology), ATG7 antibody (1:1000; Cat# 8558; Cell Signaling Technology), and GAPDH antibody (1:5000; Cat# 60004–1-Ig; Proteintech). Then, the membrane was incubated with secondary antibodies. Finally, proteins were visualized using the ChemiDoc Imaging System (Bio-Rad, Hercules, California, USA) and quantified by Image J (1.6.0) software.

2.9. Data analysis

All data were shown as means ± standard error of the mean (SEM) and analyzed with GraphPad Prism. A Student's t-test (two-tailed) was performed to evaluate statistical differences between FA and $PM_{2.5}$ groups. $P<0.05$ was defined as statistically significant.

3. Results

3.1. $PM_{2.5}$ concentration and components

In a previous study (Hu et al., 2023), we characterized the concentration and composition of $PM_{2.5}$ during exposure. The average daily concentrations of $PM_{2.5}$ in the FA and $PM_{2.5}$ chambers were 17.48 ± 2.40 μg/m^3 and 90.71 ± 7.99 μg/m^3, respectively. The most abundant metallic and non-metallic elements attached to $PM_{2.5}$ were Fe and S, respectively (Fig. 1A–B). The water-soluble inorganic ions with the highest concentration were SO_4^{2-} and NO_3^- (Fig. 1C).

3.2. $PM_{2.5}$ exposure induced BAT impairment in middle-aged mice

After eight weeks of $PM_{2.5}$ exposure, no notable changes in body weight were observed in mice at different life stages (Fig. 2A). Next, we collected adipose tissues from different anatomical locations (VAT, iWAT, and BAT) and found that $PM_{2.5}$ exposure did not change

the WAT (VAT and iWAT) mass and organ coefficient in mice at different life stages (Fig. 2B–E). However, BAT mass and organ coefficient in middle-aged mice exhibited a significant decrease after $PM_{2.5}$ exposure, although no changes were found in either young or adult mice (Fig. 2F–G). These findings indicate that BAT in middle-aged mice is more vulnerable to 8-week $PM_{2.5}$ exposure. Therefore, our subsequent investigations were centered on determining the impacts of $PM_{2.5}$ exposure on BAT in middle-aged mice.

In line with the results mentioned above, H&E staining revealed that $PM_{2.5}$ exposure changed the BAT morphology in middle-aged mice, as indicated by a slight reduction in average adipocyte size (Fig. 2H–I). BAT is rich in mitochondria, which are essential for BAT function, especially thermogenesis. We, therefore, employed high-resolution respirometry to determine the mitochondrial function of BAT and found that $PM_{2.5}$ exposure decreased CI and $CI\&II_P$ in BAT, although there was no statistical significance (Fig. 2J). These results indicate that $PM_{2.5}$ exposure leads to a reduction in BAT mass in middle-aged mice, accompanied by decreased adipocytes size and mitochondrial dysfunction.

3.3. $PM_{2.5}$ exposure arrested cell cycle and DNA replication in the BAT of middle-aged mice

To explore the underlying mechanism of $PM_{2.5}$-induced impairment of mitochondrial function in BAT, we performed transcriptomic sequencing in BAT. Fig. 3A–B shows the identification of 1281 DEGs, consisting of 350 up-regulated DEGs and 931 down-regulated DEGs. KEGG enrichment analysis of these DEGs revealed that signaling pathways associated with protein digestion and absorption, cell adhesion molecules, cell cycle, PI3K-Akt signaling pathway, and DNA replication were significantly down-regulated in response to $PM_{2.5}$ exposure (Fig. 3C). Furthermore, GO terms significantly enriched for down-regulated DEGs were related to cell cycle and DNA replication, such as cell cycle phase transition, cell cycle checkpoint, and DNA replication initiation in biological processes and kinetochore, condensed chromosome kinetochore, and mitotic spindle in cellular components (Fig. 3D). Consistently, GSEA revealed that $PM_{2.5}$ exposure remarkable inhibited DNA replication (Fig. 3E). In the prediction of PPI network, we used CytoHubba and MCODE plugin in Cytoscape to compute the Top 10 hub genes and critical modules, and found that the clues all pointed to cell cycle and DNA replication (Fig. 3F and G). The transcriptome analysis results suggest that cell cycle and DNA replication may play a key role in BAT mitochondrial dysfunction caused by $PM_{2.5}$ exposure.

To verify the inhibitory impacts of $PM_{2.5}$ exposure on the cell cycle in BAT, we used qRT-PCR to examine the mRNA expression of genes related to the cell cycle and demonstrated that $PM_{2.5}$ exposure slightly reduced the mRNA expression of Bub1 mitotic checkpoint serine/threonine kinase (*Bub1*), cyclin dependent kinase 1 (*Cdk1*), kinesin family member 11 (*Kif11*), and topoisomerase II alpha (*Top2a*) (Fig. 3H), which again suggested that exposure to $PM_{2.5}$ arrested cell cycle in BAT. These results confirm that $PM_{2.5}$ exposure arrests DNA replication and cell cycle in BAT of middle-aged mice.

3.4. $PM_{2.5}$ exposure evoked cellular senescence in the BAT of middle-aged mice

Cell cycle arrest is a defining sign of cellular senescence, which contributes to the impairment of tissue function and then induces metabolic diseases (Herranz and Gil, 2018; Huang et al., 2022). To demonstrate whether cellular senescence occurred in BAT after exposure to $PM_{2.5}$, we detected the expression of β-Gal, a marker of cellular senescence. Immunohistochemistry revealed a significantly elevated expression of β-Gal in BAT after $PM_{2.5}$ exposure (Fig. 4A–B). In addition, a notable increase in β-Gal expression induced by $PM_{2.5}$ exposure was confirmed with immunoblotting (Fig. 4C). These findings suggest that $PM_{2.5}$ exposure leads to an increased accumulation of senescent cells in the BAT of middle-aged mice.

To explore the underlying mechanism by which $PM_{2.5}$ exposure induced cell cycle arrest and cellular senescence in the BAT of middle-aged mice, we focused on the PI3K-Akt signaling pathway, which was significantly inhibited in response to $PM_{2.5}$ exposure according to the results of KEGG enrichment analysis (Fig. 3C). Moreover, AKT signaling has been shown to be involved in cell proliferation and aging (Jiang et al., 2022; Koeberle et al., 2013; Zhang et al., 2022). Next, we used immunoblotting to verify the AKT signaling and found that $PM_{2.5}$ exposure significantly inhibited phosphorylation of AKT in the BAT of middle-aged mice (Fig. 4D). These findings suggest that inhibition of the AKT signaling pathway may be involved in $PM_{2.5}$-induced cell cycle arrest and cellular senescence.

3.5. $PM_{2.5}$ exposure led to apoptosis and autophagy in the BAT of middle-aged mice

Cellular senescence has been demonstrated to have complex interactions with apoptosis and autophagy homeostasis (Banimohamad--Shotorbani et al., 2020; Kang and Elledge, 2016). In addition, the PI3K-Akt signaling pathway is also involved in regulating cell death (Jung et al., 2019; Zhang et al., 2022). To explore whether the apoptosis and autophagy homeostasis in the BAT were disrupted under the state of $PM_{2.5}$-induced senescent cell accumulation, the expression of marker genes associated with apoptosis and autophagy was detected. As shown in Fig. 5A, the mRNA expression of BCL2-associated X protein (*Bax*) and *caspase 3*, pro-apoptotic marker genes, was significantly elevated in the BAT of middle-aged mice exposed to $PM_{2.5}$. Furthermore, the expression of ATG5 was notably elevated at both the transcriptional and translational levels after $PM_{2.5}$ exposure, although no changes in the ATG7 expression and conversion from LC3I to LC3II were observed (Fig. 5A–D). These findings indicate that apoptosis and autophagy were activated in BAT of middle-aged mice under senescent cell accumulation induced by $PM_{2.5}$ exposure.

4. Discussion

The current study detected that mice in middle age were more susceptible to 8-week exposure to ambient $PM_{2.5}$ in BAT. Our main findings are as follows: (1) $PM_{2.5}$ exposure caused altered morphology and impaired mitochondrial function in BAT of middle-aged mice. (2) $PM_{2.5}$ exposure increased cellular senescence, accompanied by cell cycle arrest, impaired DNA replication, and inhibited AKT signaling pathway in BAT of middle-aged mice. (3) $PM_{2.5}$ exposure activated apoptosis and autophagy in BAT of middle-aged mice.

In line with our previous findings that hepatic lipid metabolism in middle-aged mice was more vulnerable to $PM_{2.5}$ exposure, we identified that $PM_{2.5}$ exposure caused BAT impairment in middle-aged mice, while no such effects were observed in young or adult mice. After eight weeks of exposure to $PM_{2.5}$, BAT mass and organ coefficient were significantly decreased in middle-aged mice, accompanied by mitochondrial respiratory dysfunction, indicating impaired BAT metabolism. Consistently, our prior research and other studies have found that $PM_{2.5}$ exposure led to a decrease in BAT mass, with a significant reduction in mitochondrial number and size, suggesting the loss of metabolic capacity of brown adipocytes (Della Guardia and Shin, 2022b; Xu et al., 2011). In addition, we observed that $PM_{2.5}$ exposure caused the decreased size of adipocytes of BAT. Contrary to the present finding, other studies have shown that $PM_{2.5}$ exposure induced brown adipocyte swelling in BAT (Della Guardia and Shin, 2022b; Song et al., 2020). The reason for this difference may be related to $PM_{2.5}$ exposure time and the age of the mice, which needs to be elucidated in further investigations.

A novelty of the study is that $PM_{2.5}$ exposure induced cellular senescence in BAT of middle-aged mice, evidenced by impaired DNA replication and cell cycle arrest. The cell cycle is mainly classified into the following stages: G1, S, G2, and M phase, which are mainly controlled by two events: DNA replication during the S phase and mitosis during the M phase (Matthews et al., 2022; Mei and Cook, 2021). The main molecules related to the cell cycle, including TOP2A (a DNA topoisomerase that is related to DNA replication, transcription, recombination, and mitosis (Singh et al., 2023), BUB1 (a mitotic checkpoint protein that is required for the viability of proliferating cells and the accurate segregation of chromosomes during cell division (Mishra et al., 2023; Ricke et al., 2012)), CDK1 (a master modulator that drives cells through the G2 phase and mitosis (Diril et al., 2012)), and KIF11 (a known mitotic regulator that promotes bipolar spindle formation and chromosome movement (Wang et al., 2020)). As expected, these markers of DNA replication and mitosis in BAT of middle-aged mice declined after exposure to $PM_{2.5}$. Cellular senescence, initially characterized by Hayflick as a prolonged cessation of the cell cycle, is a process that strengthens with age and leads to age-related diseases (Hayflick and Moorhead, 1961; Ogrodnik et al., 2019). We found a notable increase in β-Gal expression, a gold marker for senescent cells, indicating increased cellular senescence in BAT of middle-aged mice after $PM_{2.5}$ exposure. Similarly, limited studies found that $PM_{2.5}$ exposure increased senescence and mitochondrial damage in Human HaCaT keratinocytes and mouse skin tissues (Herath et al., 2022; Ryu et al., 2019). Mechanistically, we found that $PM_{2.5}$ exposure inhibited AKT signaling, a key regulator of cell proliferation and aging (Jiang et al., 2022; Koeberle et al., 2013; Zhang et al., 2022). Consistent with our results, Xu et al. also found that $PM_{2.5}$ exposure decreased the phosphorylation of AKT in the BAT of mice, but they linked this change to $PM_{2.5}$-induced insulin resistance (Xu et al., 2011). Therefore, further exploring the role of AKT signaling in $PM_{2.5}$-induced cellular senescence of BAT in the future is of great significance for understanding the metabolic effects of $PM_{2.5}$ exposure. Taken together, the inhibited AKT signaling, impaired DNA replication, cell cycle arrest, and cellular senescence are important events in $PM_{2.5}$-induced BAT dysfunction in middle-aged mice, which may be the important reason for the reduction in brown adipocyte size mentioned above.

Cell senescence could induce double-edged effects. On the one hand, senescent cells are essential for some physiological and pathological processes, such as embryogenesis, tumor suppression, host immunity, and tissue repair. On the other hand, the excessive accumulation of senescent cells could induce adverse consequences, such as chronic inflammation and age-related diseases (Calcinotto et al., 2019; He and Sharpless, 2017; van Deursen, 2014). In addition to quitting the cell cycle, senescent cells undergo various phenotypic changes, such as autophagy modulation (Herranz and Gil, 2018). In our study, we found that $PM_{2.5}$ exposure activated autophagy in BAT of middle-aged mice. Interestingly, autophagy is tightly regulated by mitosis. Cell cycle-related genes CKD1 and BUB1 have been demonstrated to inhibit autophagy (Li and Zhang, 2017; Odle et al., 2021; Szyniarowski et al., 2011), which is consistent with reduced expression of CDK1 and BUB1 and elevated expression of ATG5 in the current study. Furthermore, TP53 activation initiates cell cycle arrest and simultaneously activates the transcription of genes related to autophagy, such as ATG5 and ATG7, during cellular senescence, again suggesting the interaction between autophagy activation and cellular senescence (Kang and Elledge, 2016).

Apoptosis, along with autophagy, is another extensively investigated type of programmed cell death essential for mitochondrial and cell homeostasis (Vicencio et al., 2008). We found increased levels of apoptosis manifested as increased expression of apoptosis-related markers (*Bax* and *caspase 3*) in the BAT of middle-aged mice. Although senescent cells are remarkably resistant to apoptosis (Anerillas et al., 2022; Salminen et al., 2011), many classic apoptotic signals have also been found to be complexly interweaved with autophagy regulation (Mariño et al., 2014). In fact, stimuli that induce apoptosis could also induce autophagy (Pattingre et al., 2009; Yu et al., 2004). In addition, since AKT has been shown to increase cell survival by inhibiting apoptosis, the inhibition of AKT signaling caused by $PM_{2.5}$ exposure may also be a potential reason for the enhancement of apoptosis (Jung et al., 2019; Zhang et al., 2022). Although the exact intertwining regulation between autophagy, apoptosis, and senescence remains to be further explored, it did not prevent us from concluding that the cell senescence-initiated disturbance of autophagy and apoptosis contributed to mitochondrial dysfunction in BAT of middle-aged mice exposed to $PM_{2.5}$.

However, the present study has several limitations. Firstly, although the analysis included various components of $PM_{2.5}$, the one that caused mitochondrial dysfunction in BAT of middle-aged mice is still unknown. Secondly, our previous study has demonstrated the sex-dependent impacts of $PM_{2.5}$ exposure on metabolism (Li et al., 2020). Given that current findings are all from male animals, it is uncertain if the impairment of BAT mitochondrial function caused by $PM_{2.5}$ applies to females. It is imperative to explore further the sex difference after $PM_{2.5}$ exposure in the future. Thirdly, although we put forth cellular senescence and arrested cell cycle in BAT of middle-aged mice, the in-depth mechanism remains unclear and needs further investigation.

5. Conclusions

In summary, inhalation exposure to ambient $PM_{2.5}$ caused mitochondrial dysfunction in the BAT of middle-aged male mice, accompanied by increased senescent cell burden and disruption of homeostasis in apoptosis and autophagy (Fig. 6). These findings uncover the

potential etiology for the BAT dysfunction-induced by $PM_{2.5}$ exposure from the perspective of cellular senescence and imply that targeting senescent cells in BAT could be a promising strategy to counter $PM_{2.5}$-induced metabolic disorders.

Acknowledgments

This work was supported by Key Research and Development International Cooperation Projects (2019YFE0114500), National Natural Science Foundation of China (grant number 82273590, 81973001, 82173480, 81904027, 82004143). The authors acknowledge that the graphic abstract was created with Biorender.com.

Data availability

Data will be made available on request.

Abbreviations:

AKT	Protein kinase B
Atg5/7	Autophagy related 5/7
BAT	Brown adipose tissue
Bax	BCL2-associated X protein
Bub1	Bub1 mitotic checkpoint serine/threonine kinase
Cdk1	Cyclin dependent kinase 1
CI_L	Complex I LEAK respiration
CI_P	OXPHOS capacity of Complex I
$CI\&II_E$	Electron transfer system capacity of Complex I and II
$CI\&II_P$	OXPHOS capacity of Complex I and II
CII_E	Electron transfer system capacity of Complex II
DEGs	Differentially expressed genes
ETS	Electron transfer system
FA	Filtered air
Gapdh	Glyceraldehyde-3-phosphate dehydrogenase
GO	Gene Ontology
GSEA	Gene set enrichment analysis
H&E	Hematoxylin and eosin
IWAT	Inguinal white adipose tissue

KEGG	Kyoto Encyclopedia of Genes
Kif11	Kinesin family member 11
MCODE	Molecular Complex Detection
O2k	Oxygraph-2k
$PM_{2.5}$	Fine particulate matter
PPI	Protein-protein interaction
SEM	Standard error of the mean
Top2a	Topoisomerase II alpha
VAT	Visceral adipose tissue
β-Gal	Beta-galactosidase

References

Anerillas C, Herman AB, Munk R, Garrido A, et al. , 2022. A BDNF-TrkB autocrine loop enhances senescent cell viability. Nat. Commun 13, 6228. 10.1038/s41467-022-33709-8. [PubMed: 36266274]

Araviiskaia E, Berardesca E, Bieber T, Gontijo G, et al. , 2019. The impact of airborne pollution on skin. J. Eur. Acad. Dermatol. Venereol 33, 1496–1505. 10.1111/jdv.15583. [PubMed: 30897234]

Bader GD, Hogue CW, 2003. An automated method for finding molecular complexes in large protein interaction networks. BMC Bioinforma. 4, 2. 10.1186/1471-2105-4-2.

Banimohamad-Shotorbani B, Kahroba H, Sadeghzadeh H, Wilson DM 3rd, et al. , 2020. DNA damage repair response in mesenchymal stromal cells: From cellular senescence and aging to apoptosis and differentiation ability. Ageing Res Rev. 62, 101125 10.1016/j.arr.2020.101125. [PubMed: 32683038]

Calcinotto A, Kohli J, Zagato E, Pellegrini L, et al. , 2019. Cellular Senescence: Aging, Cancer, and Injury. Physiol. Rev 99, 1047–1078. 10.1152/physrev.00020.2018. [PubMed: 30648461]

Chen C, Chen H, Zhang Y, Thomas HR, et al. , 2020. TBtools: an integrative toolkit developed for interactive analyses of big biological data. Mol. Plant 13, 1194–1202. 10.1016/j.molp.2020.06.009. [PubMed: 32585190]

Della Guardia L, Shin AC, 2022a. PM(2.5)-induced adipose tissue dysfunction can trigger metabolic disturbances. Trends Endocrinol. Metab 33, 737–740. 10.1016/j.tem.2022.08.005. [PubMed: 36175280]

Della Guardia L, Shin AC, 2022b. White and brown adipose tissue functionality is impaired by fine particulate matter (PM(2.5) exposure. J. Mol. Med (Berl.) 100, 665–676. 10.1007/s00109-022-02183-6. [PubMed: 35286401]

van Deursen JM, 2014. The role of senescent cells in ageing. Nature 509, 439–446. 10.1038/nature13193. [PubMed: 24848057]

Diril MK, Ratnacaram CK, Padmakumar VC, Du T, et al. , 2012. Cyclin-dependent kinase 1 (Cdk1) is essential for cell division and suppression of DNA re-replication but not for liver regeneration. Proc. Natl. Acad. Sci. USA 109, 3826–3831. 10.1073/pnas.1115201109. [PubMed: 22355113]

Fan W, Si Y, Xing E, Feng Z, et al. , 2023. Human epicardial adipose tissue inflammation correlates with coronary artery disease. Cytokine 162, 156119. 10.1016/j.cyto.2022.156119. [PubMed: 36603481]

GBD 2015 Risk Factors Collaborators, 2016. Global, regional, and national comparative risk assessment of 79 behavioural, environmental and occupational, and metabolic risks or clusters

of risks, 1990–2015: a systematic analysis for the Global Burden of Disease Study 2015. Lancet 388, 1659–1724. 10.1016/s0140-6736(16)31679-8. [PubMed: 27733284]

Gu Y, Hao S, Liu K, Gao M, et al. , 2022. Airborne fine particulate matter (PM(2.5)) damages the inner blood-retinal barrier by inducing inflammation and ferroptosis in retinal vascular endothelial cells. Sci. Total Environ 838, 156563 10.1016/j.scitotenv.2022.156563. [PubMed: 35690207]

Hamann A, Flier JS, Lowell BB, 1996. Decreased brown fat markedly enhances susceptibility to diet-induced obesity, diabetes, and hyperlipidemia. Endocrinology 137, 21–29. 10.1210/endo.137.1.8536614. [PubMed: 8536614]

Hayflick L, Moorhead PS, 1961. The serial cultivation of human diploid cell strains. Exp. Cell Res 25, 585–621. 10.1016/0014-4827(61)90192-6. [PubMed: 13905658]

He S, Sharpless NE, 2017. Senescence in Health and Disease. Cell 169, 1000–1011. 10.1016/j.cell.2017.05.015. [PubMed: 28575665]

Herath H, Piao MJ, Kang KA, Zhen AX, et al. , 2022. Hesperidin Exhibits Protective Effects against PM(2.5)-Mediated Mitochondrial Damage, Cell Cycle Arrest, and Cellular Senescence in Human HaCaT Keratinocytes. Molecules 27. 10.3390/molecules27154800.

Herranz N, Gil J, 2018. Mechanisms and functions of cellular senescence. J. Clin. Invest 128, 1238–1246. 10.1172/jci95148. [PubMed: 29608137]

Hu R, Zhang L, Qin L, Ding H, et al. , 2023. Airborne PM(2.5) pollution: A double-edged sword modulating hepatic lipid metabolism in middle-aged male mice. Environ. Pollut 324, 121347 10.1016/j.envpol.2023.121347. [PubMed: 36858098]

Huang W, Hickson LJ, Eirin A, Kirkland JL, et al. , 2022. Cellular senescence: the good, the bad and the unknown. Nat. Rev. Nephrol 18, 611–627. 10.1038/s41581-022-00601-z. [PubMed: 35922662]

Jiang B, Wu X, Meng F, Si L, et al. , 2022. Progerin modulates the IGF-1R/Akt signaling involved in aging. eabo0322 Sci. Adv 8. 10.1126/sciadv.abo0322.

Jung SH, Lee M, Park HA, Lee HC, et al. , 2019. Integrin α6β4-Src-AKT signaling induces cellular senescence by counteracting apoptosis in irradiated tumor cells and tissues. Cell Death Differ. 26, 245–259. 10.1038/s41418-018-0114-7. [PubMed: 29786073]

Kang C, Elledge SJ, 2016. How autophagy both activates and inhibits cellular senescence. Autophagy 12, 898–899. 10.1080/15548627.2015.1121361. [PubMed: 27129029]

Kang KA, Piao MJ, Fernando P, Herath H, et al. , 2023. Korean red ginseng attenuates particulate matter-induced senescence of skin keratinocytes. Antioxid. (Basel) 12. 10.3390/antiox12081516.

Khosla S, Farr JN, Tchkonia T, Kirkland JL, 2020. The role of cellular senescence in ageing and endocrine disease. Nat. Rev. Endocrinol 16, 263–275. 10.1038/s41574-020-0335-y. [PubMed: 32161396]

Koeberle A, Shindou H, Koeberle SC, Laufer SA, et al. , 2013. Arachidonoyl-phosphatidylcholine oscillates during the cell cycle and counteracts proliferation by suppressing Akt membrane binding. Proc. Natl. Acad. Sci. USA 110, 2546–2551. 10.1073/pnas.1216182110. [PubMed: 23359699]

Li J, Song Y, Shi L, Jiang J, et al. , 2023. Long-term effects of ambient PM(2.5) constituents on metabolic syndrome in Chinese children and adolescents. Environ. Res 220, 115238. 10.1016/j.envres.2023.115238. [PubMed: 36621550]

Li R, Sun Q, Lam SM, Chen R, et al. , 2020. Sex-dependent effects of ambient PM2.5 pollution on insulin sensitivity and hepatic lipid metabolism in mice. Part Fibre Toxicol. 17, 14. 10.1186/s12989-020-00343-5 https://www.ncbi.nlm.nih.gov/pubmed/32321544. [PubMed: 32321544]

Li Z, Zhang X, 2017. Kinases Involved in Both Autophagy and Mitosis. Int J. Mol. Sci 18 10.3390/ijms18091884.

Liang CS, Duan FK, He KB, Ma YL, 2016. Review on recent progress in observations, source identifications and countermeasures of PM2.5. Environ. Int 86, 150–170. 10.1016/j.envint.2015.10.016. [PubMed: 26595670]

Mariño G, Niso-Santano M, Baehrecke EH, Kroemer G, 2014. Self-consumption: the interplay of autophagy and apoptosis. Nat. Rev. Mol. Cell Biol 15, 81–94. 10.1038/nrm3735. [PubMed: 24401948]

Martin SK, Wood RD, 2019. DNA polymerase ζ in DNA replication and repair. Nucleic Acids Res 47, 8348–8361. 10.1093/nar/gkz705. [PubMed: 31410467]

Matthews HK, Bertoli C, de Bruin RAM, 2022. Cell cycle control in cancer. Nat. Rev. Mol. Cell Biol 23, 74–88. 10.1038/s41580-021-00404-3. [PubMed: 34508254]

Mei L, Cook JG, 2021. Efficiency and equity in origin licensing to ensure complete DNA replication. Biochem Soc. Trans 49, 2133–2141. 10.1042/bst20210161. [PubMed: 34545932]

Mishra D, Mishra A, Rai SN, Singh SK, et al. , 2023. In Silico Insight to Identify Potential Inhibitors of BUB1B from Mushroom Bioactive Compounds to Prevent Breast Cancer Metastasis. Front Biosci. (Landmark Ed. 28, 151. 10.31083/j.fbl2807151.

Odle RI, Florey O, Ktistakis NT, Cook SJ, 2021. CDK1, the Other 'Master Regulator' of Autophagy. Trends Cell Biol. 31, 95–107. 10.1016/j.tcb.2020.11.001. [PubMed: 33272830]

Ogrodnik M, Salmonowicz H, Jurk D, Passos JF, 2019. Expansion and Cell-Cycle Arrest: Common Denominators of Cellular Senescence. Trends Biochem Sci. 44, 996–1008. 10.1016/j.tibs.2019.06.011. [PubMed: 31345557]

Pattingre S, Bauvy C, Carpentier S, Levade T, et al. , 2009. Role of JNK1-dependent Bcl-2 phosphorylation in ceramide-induced macroautophagy. J. Biol. Chem 284, 2719–2728. 10.1074/jbc.M805920200. [PubMed: 19029119]

Ricke RM, Jeganathan KB, Malureanu L, Harrison AM, et al. , 2012. Bub1 kinase activity drives error correction and mitotic checkpoint control but not tumor suppression. J. Cell Biol 199, 931–949. 10.1083/jcb.201205115. [PubMed: 23209306]

Ryu YS, Kang KA, Piao MJ, Ahn MJ, et al. , 2019. Particulate matter-induced senescence of skin keratinocytes involves oxidative stress-dependent epigenetic modifications. Exp. Mol. Med 51, 1–14. 10.1038/s12276-019-0305-4.

Salminen A, Ojala J, Kaarniranta K, 2011. Apoptosis and aging: increased resistance to apoptosis enhances the aging process. Cell Mol. Life Sci 68, 1021–1031. 10.1007/s00018-010-0597-y. [PubMed: 21116678]

Shannon P, Markiel A, Ozier O, Baliga NS, et al. , 2003. Cytoscape: a software environment for integrated models of biomolecular interaction networks. Genome Res 13, 2498–2504. 10.1101/gr.1239303. [PubMed: 14597658]

Sharma K, Lee HH, Gong DS, Park SH, et al. , 2019. Fine air pollution particles induce endothelial senescence via redox-sensitive activation of local angiotensin system. Environ. Pollut 252, 317–329. 10.1016/j.envpol.2019.05.066. [PubMed: 31158660]

Singh V, Afshan T, Tyagi P, Varadwaj PK, et al. , 2023. Recent development of multi-targeted inhibitors of human topoisomerase II enzyme as potent cancer therapeutics. Int J. Biol. Macromol 226, 473–484. 10.1016/j.ijbiomac.2022.12.013. [PubMed: 36495993]

Song L, Jiang S, Pan K, Du X, et al. , 2020. AMPK activation ameliorates fine particulate matter-induced hepatic injury. Environ. Sci. Pollut. Res Int 27, 21311–21319. 10.1007/s11356-020-08624-4. [PubMed: 32270451]

Subramanian A, Tamayo P, Mootha VK, Mukherjee S, et al. , 2005. Gene set enrichment analysis: a knowledge-based approach for interpreting genome-wide expression profiles. Proc. Natl. Acad. Sci. USA 102, 15545–15550. 10.1073/pnas.0506580102. [PubMed: 16199517]

Szyniarowski P, Corcelle-Termeau E, Farkas T, Høyer-Hansen M, et al. , 2011. A comprehensive siRNA screen for kinases that suppress macroautophagy in optimal growth conditions. Autophagy 7, 892–903. 10.4161/auto.7.8.15770. [PubMed: 21508686]

Torres S, Fabersani E, Marquez A, Gauffin-Cano P, 2019. Adipose tissue inflammation and metabolic syndrome. The proactive role of probiotics. Eur. J. Nutr 58, 27–43. 10.1007/s00394-018-1790-2. [PubMed: 30043184]

Vicencio JM, Galluzzi L, Tajeddine N, Ortiz C, et al. , 2008. Senescence, apoptosis or autophagy? When a damaged cell must decide its path–a mini-review. Gerontology 54, 92–99. 10.1159/000129697. [PubMed: 18451641]

Wang X, Xu M, Li Y, 2022b. Adipose tissue aging and metabolic disorder, and the impact of nutritional interventions. Nutrients 14. 10.3390/nu14153134.

Wang X, Lu W, Xia X, Zhu Y, et al. , 2022a. Selenomethionine mitigate PM2.5-induced cellular senescence in the lung via attenuating inflammatory response mediated by cGAS/STING/NF-κB pathway. Ecotoxicol. Environ. Saf 247, 114266 10.1016/j.ecoenv.2022.114266. [PubMed: 36334339]

Wang Y, Smallwood PM, Williams J, Nathans J, 2020. A mouse model for kinesin family member 11 (Kif11)-associated familial exudative vitreoretinopathy. Hum. Mol. Genet 29, 1121–1131. 10.1093/hmg/ddaa018. [PubMed: 31993640]

Wiley CD, Campisi J, 2021. The metabolic roots of senescence: mechanisms and opportunities for intervention. Nat. Metab 3, 1290–1301. 10.1038/s42255-021-00483-8. [PubMed: 34663974]

Xu X, Liu C, Xu Z, Tzan K, et al. , 2011. Long-term exposure to ambient fine particulate pollution induces insulin resistance and mitochondrial alteration in adipose tissue. Toxicol. Sci 124, 88–98. 10.1093/toxsci/kfr211. [PubMed: 21873646]

Yi W, Zhao F, Pan R, Zhang Y, et al. , 2022. Associations of Fine Particulate Matter Constituents with Metabolic Syndrome and the Mediating Role of Apolipoprotein B: A Multicenter Study in Middle-Aged and Elderly Chinese Adults. Environ. Sci. Technol 56, 10161–10171. 10.1021/acs.est.1c08448. [PubMed: 35802126]

Yu L, Alva A, Su H, Dutt P, et al. , 2004. Regulation of an ATG7-beclin 1 program of autophagic cell death by caspase-8. Science 304, 1500–1502. 10.1126/science.1096645. [PubMed: 15131264]

Zhang L, Li C, Marhaba A, Zhu R, et al. , 2022. ITF2357 induces cell cycle arrest and apoptosis of meningioma cells via the PI3K-Akt pathway. Med Oncol. 40, 21. 10.1007/s12032-022-01883-w. [PubMed: 36445551]

Zhang LM, Lv SS, Fu SR, Wang JQ, et al. , 2021. Procyanidins inhibit fine particulate matter-induced vascular smooth muscle cells apoptosis via the activation of the Nrf2 signaling pathway. Ecotoxicol. Environ. Saf 223, 112586 10.1016/j.ecoenv.2021.112586. [PubMed: 34364126]

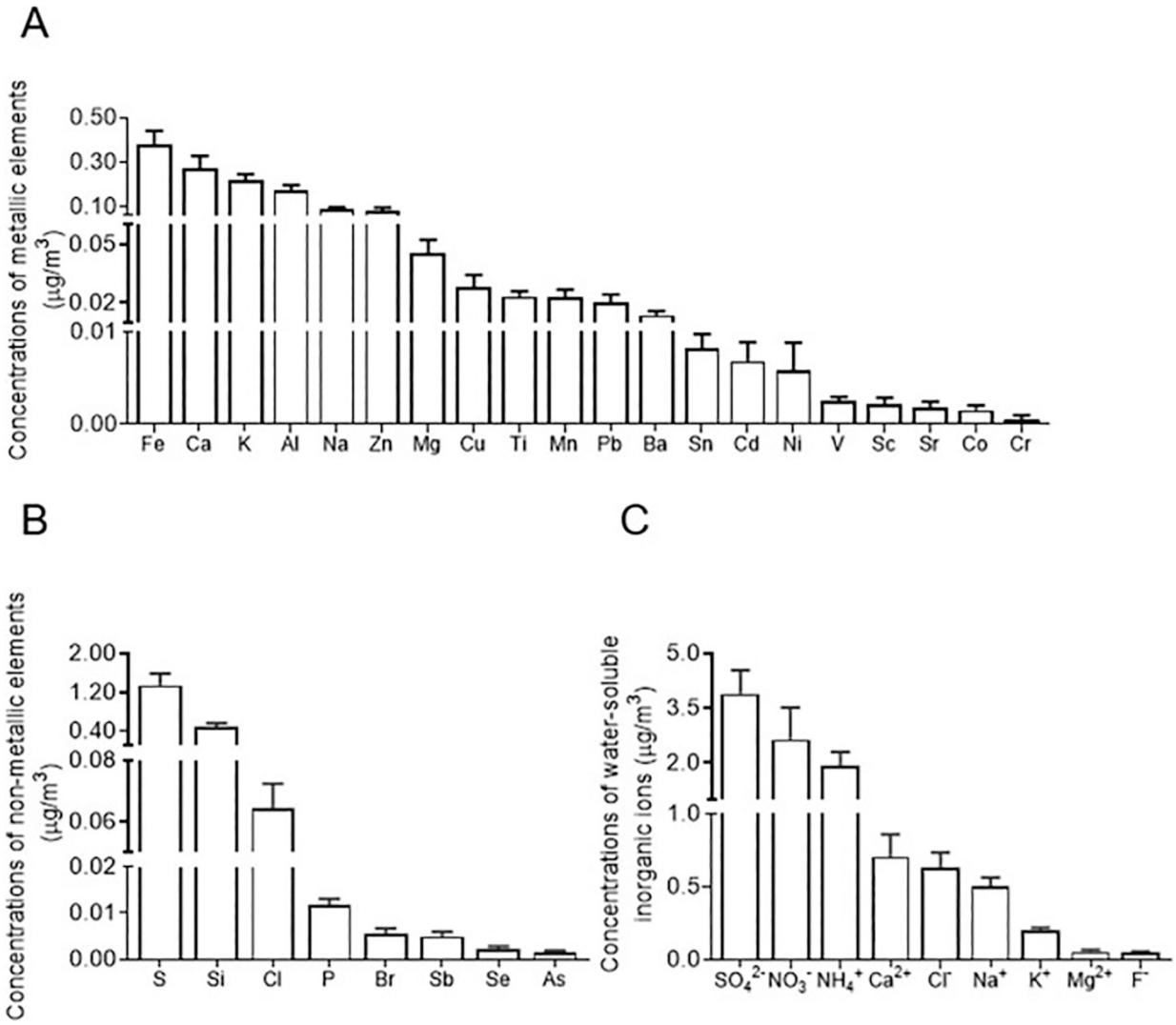

Fig. 1.

Component analysis of $PM_{2.5}$ at the study site. A-C. Concentrations of metallic element (A), non-metallic element (B), and water-soluble inorganic ions (C) in $PM_{2.5}$ during the exposure period. All data were expressed as means ± SEM. Note: $PM_{2.5}$, fine particulate matter; SEM, standard error of the mean.

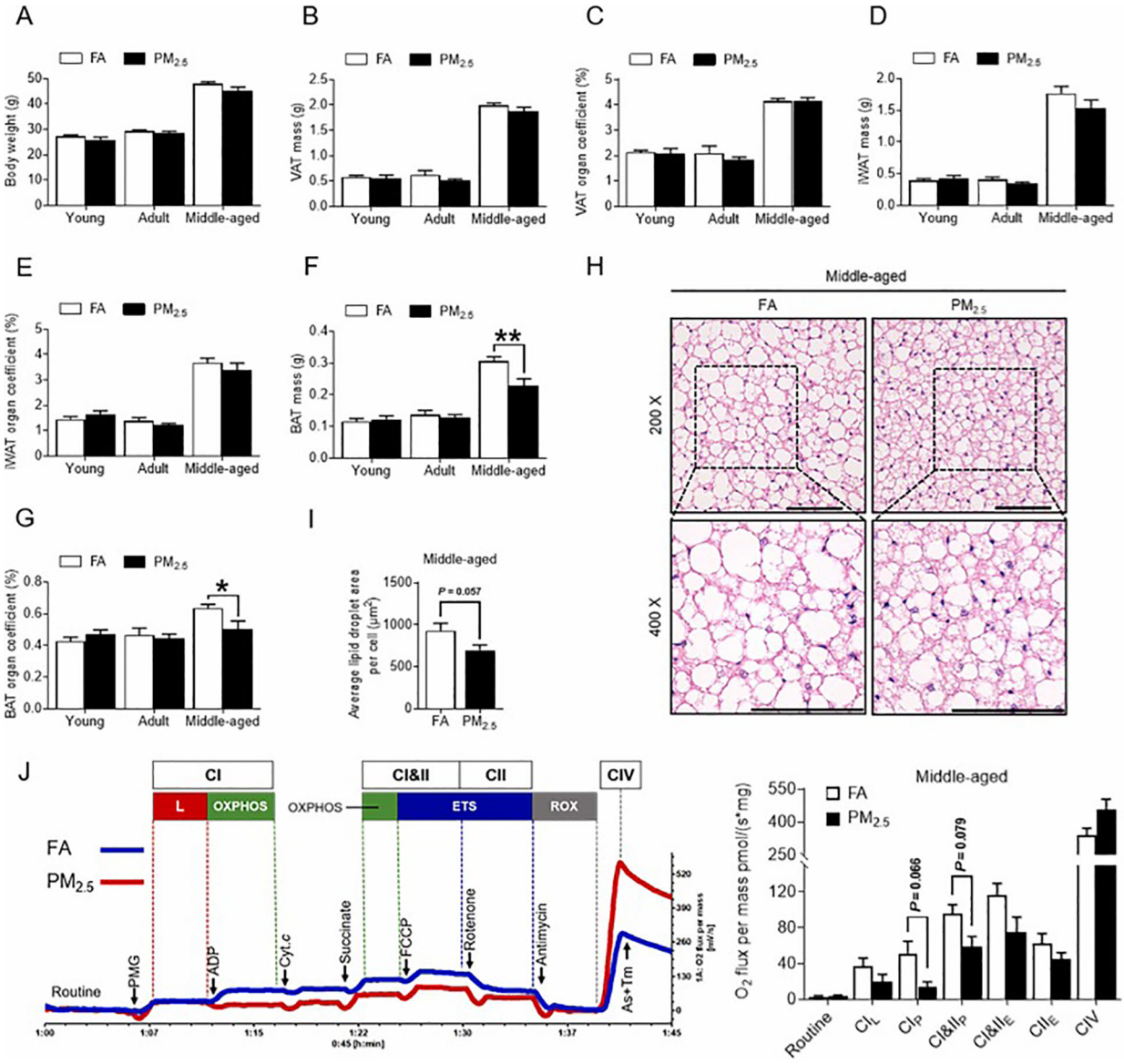

Fig. 2.

Effects of $PM_{2.5}$ exposure on body weight and BAT mass in mice at three life stages and morphology and mitochondrial function of the BAT in middle-aged mice. **A-G.** Body weight (A), VAT mass (B), VAT organ coefficient (C), iWAT mass (D), iWAT organ coefficient (E), BAT mass (F), and BAT organ coefficient (G) of mice at three life phases. H. Representative images of H&E staining (200× and 400 ×) in BAT sections of middle-aged mice; bar = 100 μm. I. The quantification of adipocyte size in H&E staining. J. Representative respirometric traces from BAT homogenates in middle-aged mice using high-resolution respirometry. All data were expressed as means ± SEM. Data were compared using Student's t-test, *p<0.05 and **p<0.01 compared to the FA group. For panels (A-G), n = 7–10 per group. For H&E staining (I), n = 7–8 per group. For high-resolution respirometry (J), n = 3 per group. Note: BAT, brown adipose tissue; CI_L, Complex I LEAK respiration; CI_P, OXPHOS capacity of Complex I; $CI\&II_P$, OXPHOS capacity of Complex I and II; $CI\&II_E$, electron transfer

system capacity of Complex I and II; CII_E, the electron transfer system capacity of Complex II; ETS, electron transfer system; FA, filtered air; H&E, hematoxylin and eosin; iWAT, inguinal white adipose tissue; $PM_{2.5}$, fine particulate matter; PMG, pyruvate, malate, and glutamate; SEM, standard error of the mean; VAT, visceral adipose tissue.

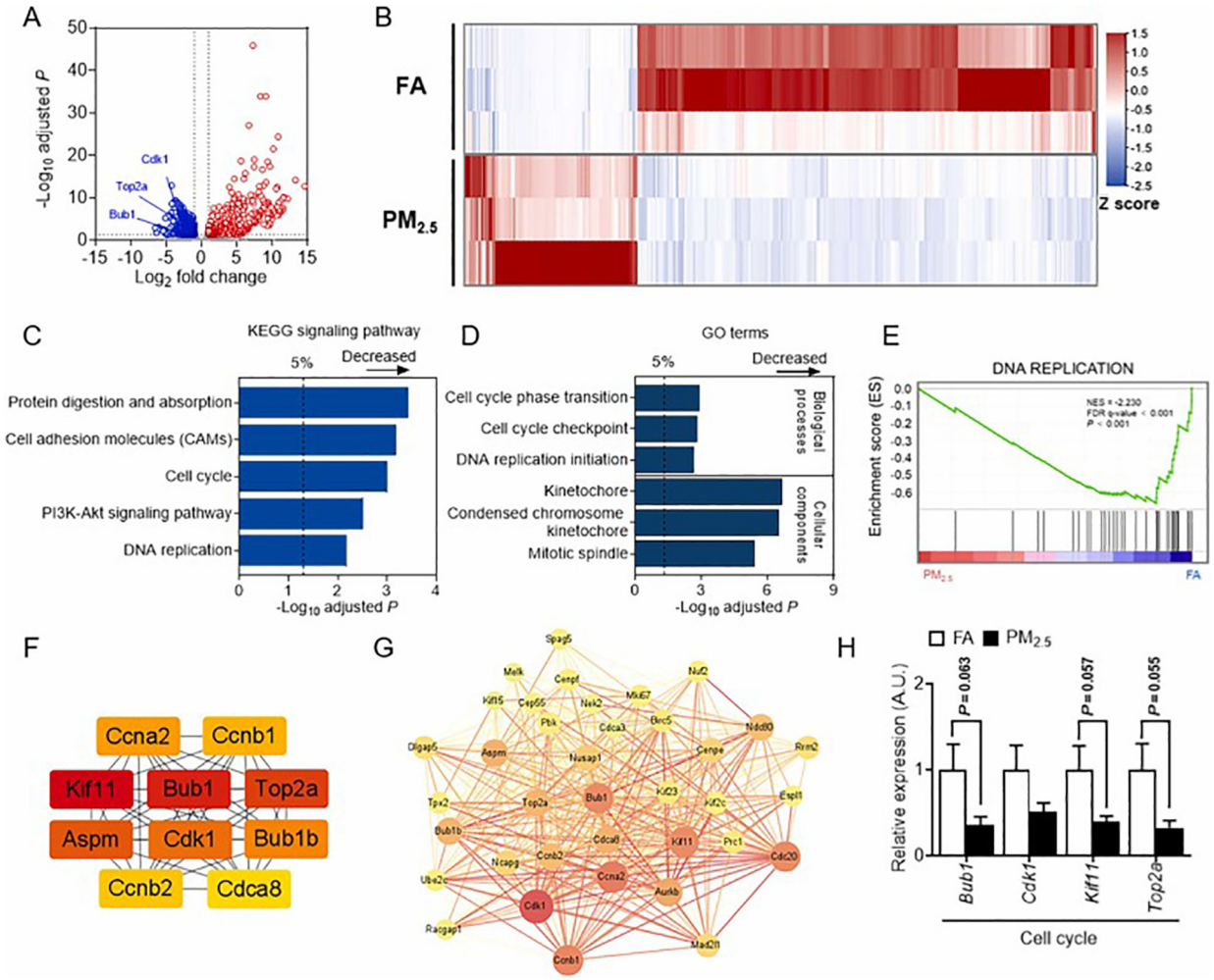

Fig. 3.

Effects of $PM_{2.5}$ exposure on cell cycle and DNA replication in the BAT of middle-aged mice. A-B. Volcano plot (A) and heatmap (B) of differentially expressed genes in BAT after eight weeks of $PM_{2.5}$ exposure. C. The decreased KEGG signaling pathways in the $PM_{2.5}$ group relative to the FA group. D. Significant down-regulated GO categories for biological processes and cellular components. E. GSEA on RNA-seq data. F. Top 10 hub genes were calculated using the CytoHubba plugin. G. The significant module related to the cell cycle was identified from the PPI network according to the MCODE method using the differentially expressed genes in BAT after eight weeks of $PM_{2.5}$ exposure. The larger the node and the redder the color, the more critical the role of the gene represented by the node; the thicker the connection between the two nodes, and the redder the color, the closer the interaction between the two genes represented by the node. H. mRNA expression of the cell cycle-related genes in the BAT of middle-aged mice. All data were expressed as means ± SEM. Data were compared using Student's t-test. For RNA-seq analysis (A-G), n = 3 per group. For detecting mRNA expression (H), n = 6 per group. Note: BAT, brown adipose tissue; *Bub1*, Bub1 mitotic checkpoint serine/threonine kinase; *Cdk1*, cyclin dependent kinase 1; FA, filtered air; GO, Gene Ontology; GSEA, gene set enrichment analysis; KEGG, Kyto Encyclopedia of Genes; *Kif11*, kinesin family member 11; MCODE,

Molecular Complex Detection; $PM_{2.5}$, fine particulate matter; SEM, standard error of the mean; *Top2a*, topoisomerase II alpha.

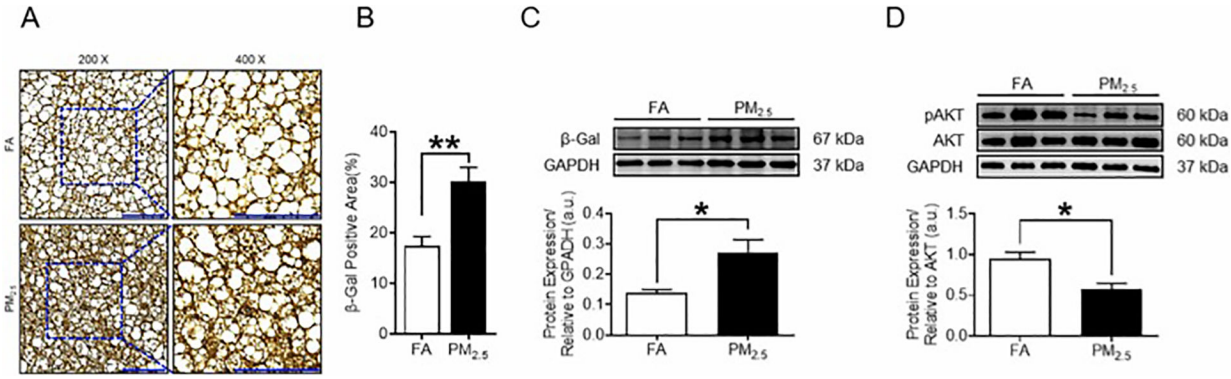

Fig. 4.

Effects of $PM_{2.5}$ exposure on cellular senescence in the BAT of middle-aged mice. **A.** Representative images of immunohistochemistry (200× and 400 ×) in BAT sections of middle-aged mice stained with β-Gal antibody; bar = 100 μm. **B.** The quantification of the positive area in immunohistochemistry. **C-D.** Representative bands and quantitative analysis of β-Gal (**C**), phosphorylated, and total AKT (**D**) in the BAT of middle-aged mice. All data were expressed as means ± SEM. Data were compared using Student's t-test, *p<0.05 and **p<0.01 compared to the FA group. For immunohistochemistry staining (B), n = 5 per group. For detecting protein expression (C-D), n = 4 per group. Note: AKT, protein kinase B; BAT, brown adipose tissue; FA, filtered air; GAPDH, glyceraldehyde-3-phosphate dehydrogenase; $PM_{2.5}$, fine particulate matter; SEM, standard error of the mean; β-Gal, beta-galactosidase.

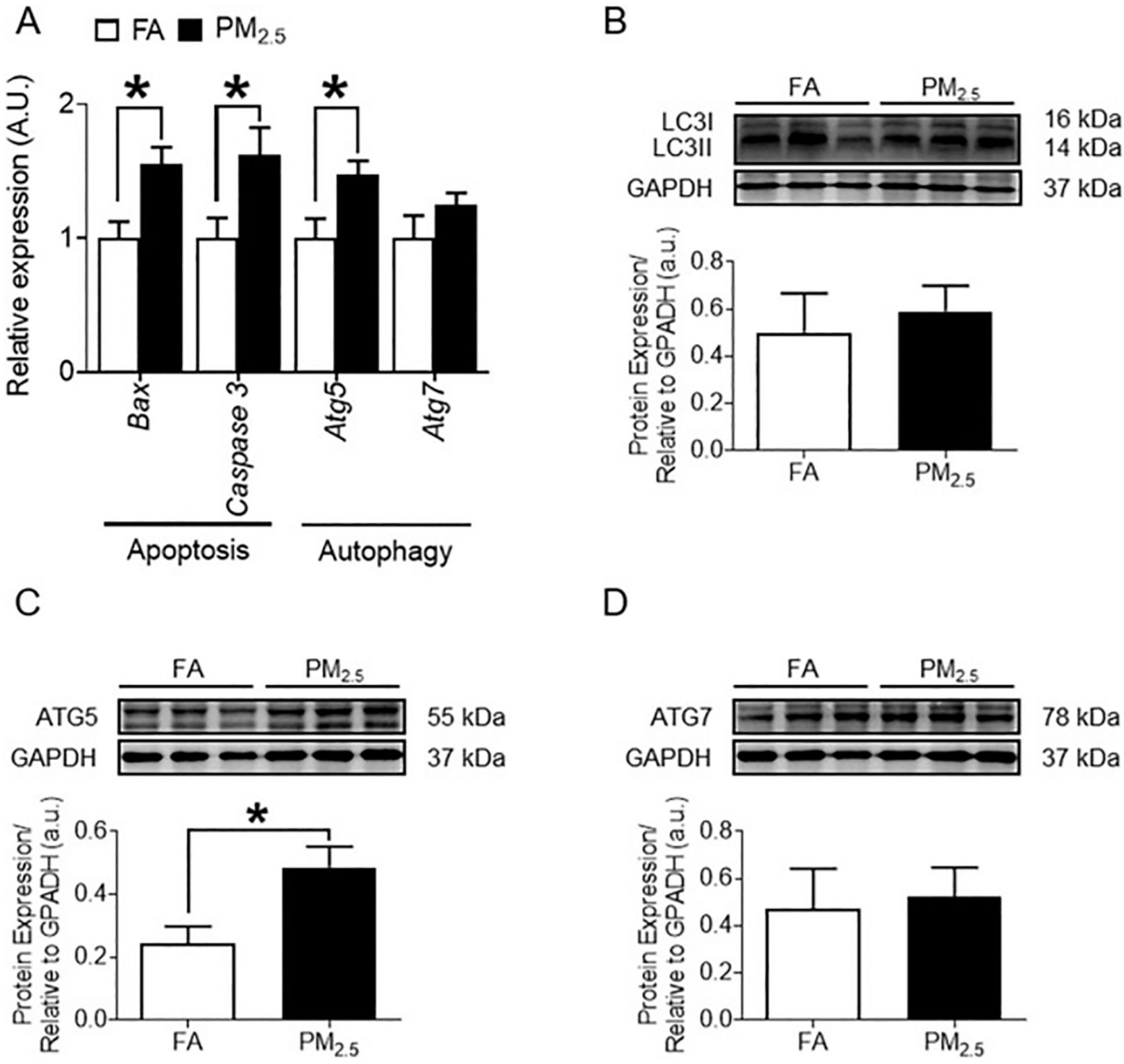

Fig. 5.

Effects of $PM_{2.5}$ exposure on autophagy and apoptosis in the BAT of middle-aged mice. A. mRNA expression of the autophagy and apoptosis-related genes in the BAT of middle-aged mice. B-D. Representative bands and quantitative analysis of LC3II (B), ATG5 (C), and ATG7 (D) in the BAT of middle-aged mice. All data were expressed as means ± SEM. Data were compared using Student's t-test, *p<0.05 and ** q<0.01 compared to the FA group. For detecting mRNA expression (A), n = 6 per group. For detecting protein expression (B-D), n = 4 per group. Note: ATG5/7, autophagy related 5/7; *Bax*, BCL2-associated X protein; BAT, brown adipose tissue; FA, filtered air; GAPDH, glyceraldehyde-3-phosphate dehydrogenase; $PM_{2.5}$, fine particulate matter; SEM, standard error of the mean.

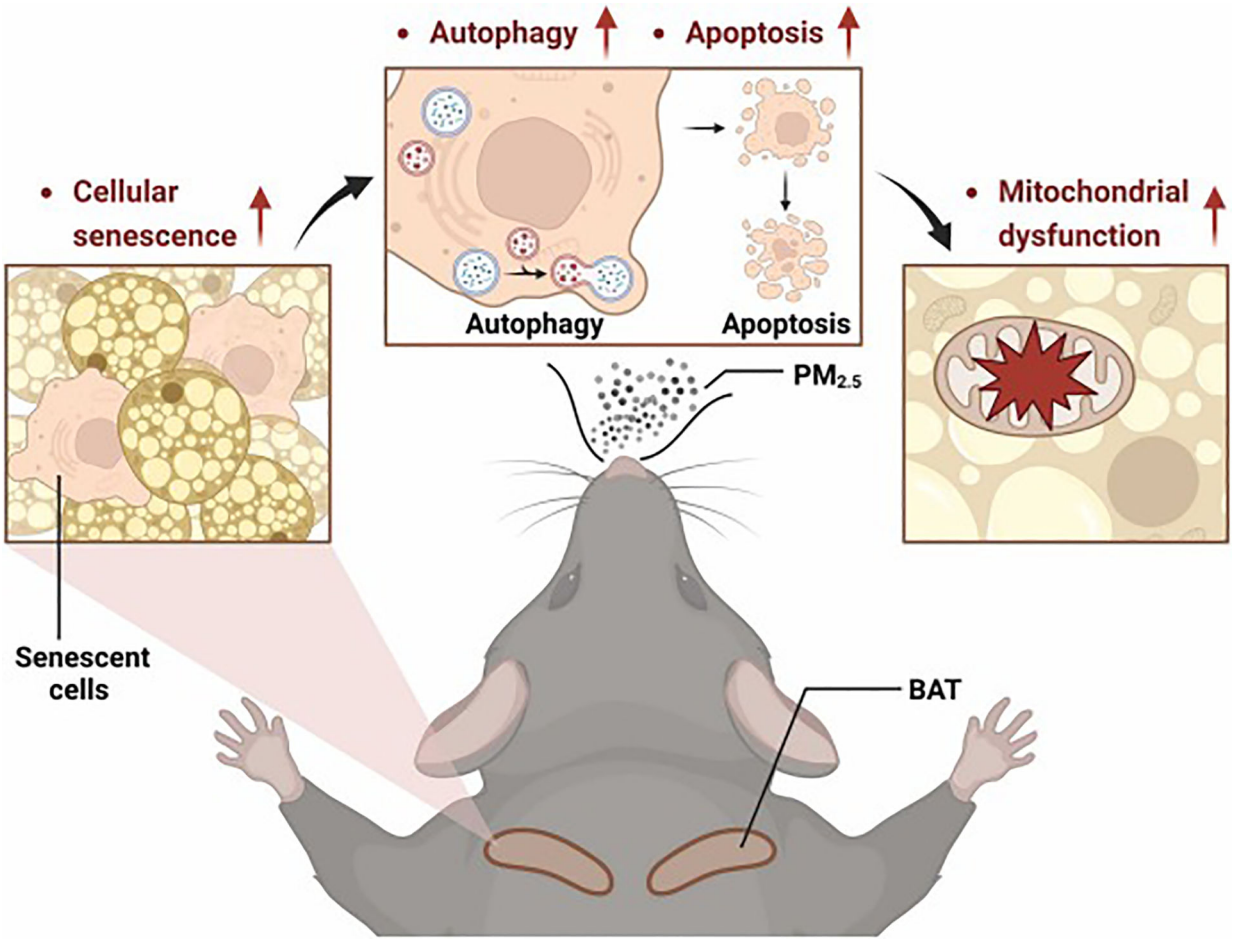

Fig. 6.

Schematic highlights that concentrated ambient $PM_{2.5}$ exposure induced cellular senescence and disrupted homeostasis in autophagy and apoptosis, ultimately causing mitochondrial dysfunction of BAT in middle-aged male mice. Note: BAT, brown adipose tissue; FA, filtered air; $PM_{2.5}$, fine particulate matter. It was created with BioRender.com.

Table 1

Primers used for qRT-PCR.

Genes	Forward primer	Reverse primer
Atg5	TGTGCTTCGAGATGTGTGGTT	ACCAACGTCAAATAGCTGACTC
Atg7	CAGAAGAAGTTGAACGAGTA	CAGAGTCACCATTGTAGTAAT
Bax	TGAAGACAGGGGCCTTTTTG	AATTCGCCGGAGACACTCG
Bub1	AGAATGCTCTGTCAGCTCATCT	TGTCTTCACTAACCCACTGCT
Caspase 3	GACTGATGAGGAGAATGGCTTG	TGCAAAGGGACTGGATGAAC
Cdk1	AGAAGGTACTTACGGTGTGGT	GAGAGATTTCCCGAATTGCAGT
Kif11	GGCTGGTATAATTCCACGCAC	CCGGGGATCATCAAACATCTG
Top2a	CAACTGGAACATATACTGCTCCG	GGGTCCCTTTGTTTGTTATCAGC
Gpadh	AGGTCGGTGTGAACGGATTTG	GGGGTCGTTGATGGCAACA

Note: *Atg5/7*, autophagy related 5/7; *Bax*, BCL2-associated X protein; *Bub1*, Bub1 mitotic checkpoint serine/threonine kinase; *Cdk1*, cyclin dependent kinase 1; *Kif11*, kinesin family member 11; *Top2a*, topoisomerase II alpha; *Gapdh*, glyceraldehyde-3-phosphate dehydrogenase.